Indian Journal of Engineering & Materials Sciences
Vol. 29, August 2022, pp. 470-480
DOI: 10.56042/ijems.v29i4.47238

Finite element analysis and optimization of active magnetic bearings for contra-rotating coaxial rotor system

Shashank Shekhar Singh*, & Punit Kumar

Department of Mechanical Engineering, National Institute of Technology Kurukshetra, Haryana 136 119, India

Received: 8 March 2021; Accepted: 17 September 2021

This paper presents the design, analysis and optimization of Active Magnetic Bearings (AMBs) to support the inner rotor in a contra-rotating coaxial rotor system. An FEM based rotordynamic model is developed using 8-dof Timoshenko beam elements assuming both inner and outer rotors to be flexible. The dynamic response of this system due to an unbalanced force is used in one of the constraints of a multi-objective genetic algorithm for controlling the vibration amplitude within 10% of the air gap. A maximum reduction of 46.9% in the amplitude peak is obtained under the present conditions. Hence, this work also offers a tool useful in touch-down bearing design. The PD controller gains are found to govern the stiffness and damping properties of the AMB. On increasing the mass unbalance by a factor of 2.5, number of turns, pole width and maximum current are found to increase by 52.9%, 29.4% and 71.67% respectively.

Keywords: Active magnetic bearing, Coaxial rotor, Genetic Algorithm, Optimization, Rotordynamics

1 Introduction

Coaxial Rotor Systems (CRSs) are widely used in aerospace industry and nuclear power plants because of their advantages over single rotor systems. For instance, in the case of helicopters, a contra-rotating CRS eliminates the need of a separate anti-torque system and at the same time, the overall system becomes more compact. Coaxial rotor system consists of inner and outer rotors which are connected by an intershaft bearing. In general, the whole system is supported by conventional bearings and dampers which provide the required stiffness and damping. Chiang *et al.*[1] modelled single and dual rotor system and predicted the natural frequencies, critical speed and bearing stiffness for different speed ratios. Ferraris *et al.*[2] studied the dynamic behaviour of non-symmetric coaxial rotors. Yang *et al.*[3] considered fixed point rubbing and studied the phenomenon of beat vibration in dual rotor system.

In recent years, active magnetic bearings (AMBs) have gained popularity over conventional bearings because AMBs not only support the load but also control the rotordynamics of the system actively through a feedback control loop. So, it is important to study the behaviour of coaxial rotor system incorporating AMBs. These bearings use attractive electromagnetic force to support the rotor and allow contactless relative motion between the rotor and the bearing. Consequently, no mechanical wear takes place and no lubrication is required during its operation.[4] Bornstein[5] developed expressions for calculating dynamic load capacity of active electromagnetic bearings. Samanta & Hirani[6] studied different radial configurations for improving the load carrying capacity and other dynamic factors of magnetic bearing. Lijesh *et al.*[7] dealt with a pragmatic optimization of axially stacked passive magnetic bearings for maximum radial load capacity. Kuppa & Lal[8] proposed a methodology for coupled turbine generator AMB system and developed a mathematical relationship for a misaligned rotor system while considering rotor imbalance. Srinivas *et al.*[9] studied misalignment in coupled rotor systems using the dynamic component of coupling stiffness. In this work, AMBs were employed as auxiliary bearings and also for condition monitoring. Zhao *et al.*[10] studied the rotordynamic behaviour for the case of vertical rotor drop, while Yulan *et al.*[11] considered horizontal rotor drop in their dynamic analysis. Moreira & Thouverez[12] studied the influence of blade flexibility in a turbomolecular pump rotor supported on AMBs.

Amongst the various optimization techniques available in literature, genetic algorithm (GA) is the most widely used technique for AMBs because of its advantages over the others. Rao & Tiwari[13] applied multiobjective genetic algorithm for the optimization

*Corresponding author (E-mail: shashank.singh1951@gmail.com)

of thrust magnetic bearings. Zhong & Palazzolo[14] optimized homopolar type magnetic bearing actuator. Lijesh & Hirani[15] considered the constraints due to bearings geometry as well as losses while optimizing an eight-pole radial active magnetic bearing. Zhong *et al.*[16] considered actuator mass, power loss and static load as the objective functions and included non-linearities in their AMB design.

From the above discussion, it follows that most of the studies on active magnetic bearings pertain to simple rotor systems and issues related to the AMBs employed in a coaxial rotor system need more attention. Therefore, the primary aim of this paper is to develop a rotordynamic model for an unbalanced contra-rotating coaxial rotor system with the inner rotor supported by AMBs. This work also aims at optimization of AMB parameters so as to minimize the overall volume, maximize the force slew rate limit and control the vibration amplitudes within 10% of the air gap for safe operation using a multi-objective genetic algorithm (MOGA). The system response and hence, vibration amplitudes are obtained using an FEM based rotordynamic analysis of the flexible coaxial rotor system.

2 Materials and Methods

2.1 AMB Design Equations and Constraints

Hetero-polar configuration of eight electromagnetic (EM) poles (4 pairs) is the most extensively used AMB design as shown in Fig. 1. In the following subsections, the various design equations and constraints used in the present analysis are presented.

2.1.1 AMB Force

The bearing force produced by an EM pair is determined as follows:[17]

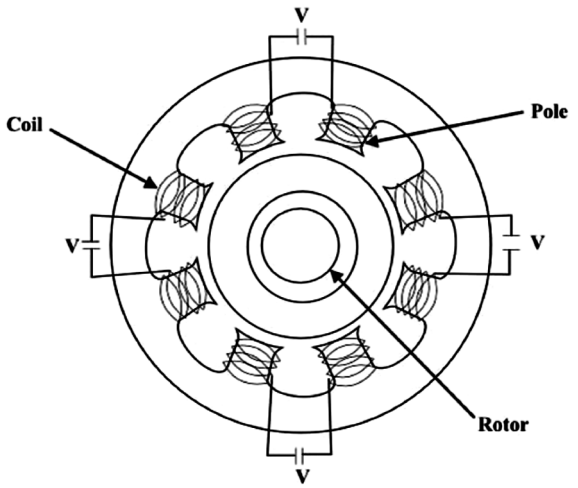

Fig. 1 — Eight-Pole Hetero-polar Active Magnetic Bearing.

$$F_n = \frac{\mu_o A_g N^2 I_n^2 \cos\alpha}{(G - d\cdot\cos\alpha)^2} \quad \ldots (1)$$

The AMB shown in Fig. 1 is so aligned with respect to the rotor system that its x and y axes are inclined at 45° to the vertical. This ensures equal static loads due to rotor weight along both the axes. Therefore, equations for only one axis (y-axis) are given in the following text. The current in addition to the bias current to support the applied load component in y direction is expressed as:

$$i_y = I_{stat} + I_{y,dyn} \quad \ldots (2)$$

The resultant bearing force is:

$$P_{y,brg} = \mu_o A_g N^2 \cos\alpha \left\{ \left(\frac{I_b + I_{stat} + I_{y,dyn}}{G - y\cos\alpha} \right)^2 - \left(\frac{I_b - I_{stat} - I_{y,dyn}}{G + y\cos\alpha} \right)^2 \right\} \quad \ldots (3)$$

The above bearing force is linearized using Taylor expansion:[17]

$$P_{y,brg} = P_{stat} + K_i I_{y,dyn} + K_{y,d} y = P_{stat} + P_{y,dyn} \quad \ldots (4)$$

where,

$$P_{stat} = \frac{4\mu_o A_g N^2 \cos\alpha}{G^2} I_b I_{stat} \quad \ldots (5)$$

$$K_i = \frac{4\mu_o A_g N^2 \cos\alpha}{G^2} I_b \quad \ldots (6)$$

$$K_{y,d} = \frac{4\mu_o A_g N^2 \cos^2\alpha}{G^3} \left(I_b^2 + I_{stat}^2 \right) \quad \ldots (7)$$

2.1.2 Design Constraints

The various design parameters considered in this study should satisfy the following constraints:

Constraint 1: Stability Constraint

The force acting on the rotor due to the AMB is given by:

$$F_{AMB} = K_i i + K_d x \quad \ldots (8)$$

where,

$$i = -G_s G_d \left(k_p x + k_d \dot{x} \right) \quad \ldots (9)$$

Therefore,

$$F_{AMB} + K_i G_s G_d k_d \dot{x} + \left(K_i G_s G_d k_p - K_d \right) x = 0 \quad \ldots (10)$$

To ensure the stability of the whole system,

$$k_d \geq 0 \text{ and } k_p > \frac{K_d}{K_i G_s G_d} \quad \ldots (11)$$

Constraint 2: Power Supply Voltage Constraint

The inductance of an EM coil is defined as:

$$L_c = \frac{2N\phi}{I} = \frac{2\mu_o A_g N^2}{G} \quad \text{... (12)}$$

The bias and control voltages are determined as follows:

$$V_b = I_b R_c + I_{stat} R_c \text{ and } V_c = I_{dyn}\left(L_c\omega\right)\sqrt{1+\left(R_c / L_c\omega\right)^2} \quad \text{... (13)}$$

Constraint 3: Maximum Current Constraint

$$V_p \geq V_b + V_c \quad \text{... (14)}$$

The maximum current flow depends on the current density of the wire material

$$I_{\max} < \zeta\left(\pi d_c^2/4\right) \quad \text{... (15)}$$

where, ζ is the maximum current density in copper wire.

Constraint 4: Flux Density Constraint

The flux density in the air-gap is given by:[17]

$$B_g = \frac{\mu_o NI}{G} \quad \text{... (16)}$$

Equating the flux in the air gap and core:

$$B_g = \frac{\mu_o NI}{G} \text{ and } B_c = c\frac{\mu_o NI}{G} \quad \text{... (17)}$$

where, $c = \frac{A_g}{A_c}$.

To avoid saturation of the magnetic material, the following constraint must be satisfied:

$$B_c \leq B_{sat} \quad \text{... (18)}$$

Constraint 5: Winding Space Constraint

$$A_r \leq A_w \quad \text{... (19)}$$

where,

$$A_w = 0.8\left(l\cos\alpha\right)\left[\left(d_p + 2s + l\right)\sin\alpha - W_m\cos\alpha\right] \quad \text{... (20)}$$

and

$$A_r = 2N\frac{\pi\left(d_c + d_t\right)^2}{4} \quad \text{... (21)}$$

Constraint 6: Maximum Rotor Response Constraint

$$\text{Max}\left\{R_{AMB}\right\} < 0.1G \quad \text{... (22)}$$

Constraint 7: Linear Control Current Constraint

$$i_{c,\max} \leq G_s k_p G_d \left(YG\right)_{\max} \quad \text{... (23)}$$

Constraint 8: Maximum Sleeve Length Constraint

$$\frac{A_g}{W_m} \leq b_{\max} \quad \text{... (24)}$$

Constraint 9: Maximum Diameter of Stator Constraint

$$D_{stator} = d_p + 2\left(s + l + 1.1W_m\right) \leq D_{\max} \quad \text{... (25)}$$

Constraint 10: Pole Width Constraint

$$0.6W_m \leq \left(0.5d_p\sin\alpha - 1.5G\cos\alpha\right) \quad \text{... (26)}$$

2.1.3 Performance Evaluation

Force Slew Rate Limitation

The slew rate of the magnetic force is:[17]

$$\left.\frac{dP_{y,brg}}{dt}\right|_{y=0} = K_i\frac{di_y}{dt} \quad \text{... (27)}$$

Using the above equations:

$$\max\left\{\left.\frac{dP_{y,brg}}{dt}\right|_{y=0}\right\} = \frac{\beta}{\beta+1}\cdot\frac{2B_{sat}\cos\alpha}{c\mu_o N}\cdot\frac{V_c}{\sqrt{1+\left(R_c / L_c\omega\right)^2}} \quad \text{... (28)}$$

Bearing Volume

The overall bearing volume is given as

$$V_{brg} = \frac{\pi D_{stat}^2 b}{4} \quad \text{... (29)}$$

2.1.4 Design-Optimization Algorithm

The step-by-step procedure for preliminary design and optimization of a radial active magnetic bearing system is given below:

a) Estimate the maximum static and dynamic load capacity per bearing axis and hence, $P_{\max}$.

b) Estimate the maximum current ($I_{\max}$) on the basis of Eq. (15) and using it, estimate the number of turns (N) as follows:

$$N = \frac{B_{\max} G}{\mu_o I_{\max} c} \quad \text{... (30)}$$

c) Calculate the required air gap area as follows:

$$A_g = \frac{P_{\max} G^2}{4\mu_o N^2 I_b\, i_{c,\max}\cos\alpha} \quad \text{... (31)}$$

where,

$$I_b = \frac{\beta}{\beta+1} I_{\max} \quad \text{... (32)}$$

and

$$i_{c,\max} = \frac{1}{\beta+1} I_{\max} \quad \text{... (33)}$$

d) Assign suitable values to the design variables w_m, l, k_p and k_d.

e) Calculate the sleeve length as follows:

$$b = \frac{A_g}{w_m} \quad \text{... (34)}$$

f) Using the current values of design variables, calculate the objective functions f_1 and f_2, i.e., the limiting force slew rate and bearing volume from Eqs. (28) and (29) respectively. In this optimization problem, it is required to maximize the force slew rate and minimize the bearing volume.

g) Calculate the composite normalized objective function as follows:

$$f = \frac{f_1}{f_{1,0}} + \frac{f_{2,0}}{f_2} \quad \text{... (35)}$$

where, $f_{1,0}$ and $f_{2,0}$ are the reference values of objective functions 1 and 2. This objective function f is maximized subject to the design constraints using genetic algorithm with penalty based approach.

2.2 Modelling of AMB Coaxial rotor system

A typical AMBCRS, as shown in Fig. 2(a) consists of (i) inner and outer rotors (ii) disks (iii) active magnetic bearings (iv) inter-shaft bearing and (v) roller bearings. In the present study finite element method (FEM) has been incorporated for the dynamic analysis of the AMBCRS. Figure 2(b) represents discretization of the system under consideration into various elements, i.e. disks, rotor and bearings, while the local coordinates for the rotor element are shown in Fig. 2(c). The governing equation incorporating all the elements of a rotor system is given by:

$$[M]\{\ddot{q}(t)\} + [C]\{\dot{q}(t)\} + \Omega[G]\{\dot{q}(t)\} + [K]\{q(t)\} = \{F(t)\} \quad \text{... (36)}$$

where, [M], [C], [G], and [K] represents global matrices of the rotor system and *F(t)* is the force acting on the system. Elements matrices which contribute to system global matrices are discussed in the following subsections.

2.2.1 Bearing Stiffness and Damping Matrix

The contribution of bearings to the equation of motion is expressed as follows:

$$[C_{be}]\{\dot{q}_{be}(t)\} + [K_{be}]\{q_{be}(t)\} = \{F_{be}(t)\} \quad \text{... (37)}$$

where,

$$[K_{be}] = \begin{bmatrix} k_{be_{xx}} & k_{be_{xy}} & 0 & 0 \\ k_{be_{xy}} & k_{be_{yy}} & 0 & 0 \\ 0 & 0 & 0 & 0 \\ 0 & 0 & 0 & 0 \end{bmatrix} \quad \text{... (38)}$$

$$[C_{be}] = \begin{bmatrix} c_{be_{xx}} & c_{be_{xy}} & 0 & 0 \\ c_{be_{xy}} & c_{be_{yy}} & 0 & 0 \\ 0 & 0 & 0 & 0 \\ 0 & 0 & 0 & 0 \end{bmatrix} \quad \text{... (39)}$$

$[K_{be}]$ and $[C_{be}]$ are bearing stiffness and damping matrices respectively. As inter-shaft bearing connects the inner and outer rotors, additional elements are introduced in the intershaft stiffness and damping matrices. If intershaft bearing is located at '*i*' node of inner rotor and '*j*' node of outer rotor, then intershaft bearing stiffness and damping matrices are,

$$[K_{be}^{is}] = \begin{array}{c} \\ (4i-3) \\ (4i-2) \\ (4o-3) \\ (4o-2) \end{array} \begin{array}{c} \begin{array}{cccc} (4i-3) & (4i-2) & (4o-3) & (4o-2) \end{array} \\ \begin{bmatrix} k_{be_{xx}} & k_{be_{xy}} & -k_{be_{xx}} & -k_{be_{xy}} \\ k_{be_{xy}} & k_{be_{yy}} & -k_{be_{xy}} & -k_{be_{yy}} \\ -k_{be_{xx}} & -k_{be_{xy}} & k_{be_{xx}} & k_{be_{xy}} \\ -k_{be_{xy}} & -k_{be_{yy}} & k_{be_{xy}} & k_{be_{yy}} \end{bmatrix} \end{array} \quad \text{... (40)}$$

$$[C_{be}^{is}] = \begin{array}{c} \\ (4i-3) \\ (4i-2) \\ (4o-3) \\ (4o-2) \end{array} \begin{array}{c} \begin{array}{cccc} (4i-3) & (4i-2) & (4o-3) & (4o-2) \end{array} \\ \begin{bmatrix} c_{be_{xx}} & c_{be_{xy}} & -c_{be_{xx}} & -c_{be_{xy}} \\ c_{be_{xy}} & c_{be_{yy}} & -c_{be_{xy}} & -c_{be_{yy}} \\ -c_{be_{xx}} & -c_{be_{xy}} & c_{be_{xx}} & c_{be_{xy}} \\ -c_{be_{xy}} & -c_{be_{yy}} & c_{be_{xy}} & c_{be_{yy}} \end{bmatrix} \end{array} \quad \text{... (41)}$$

and the contribution of intershaft bearing to the equation of motion is:

$$[C_{be}^{is}]\frac{d}{dt}\{q_{be}^{is}(t)\} + [K_{be}^{is}]\{q_{be}^{is}(t)\} = \{F_{be}^{is}(t)\} \quad \text{... (42)}$$

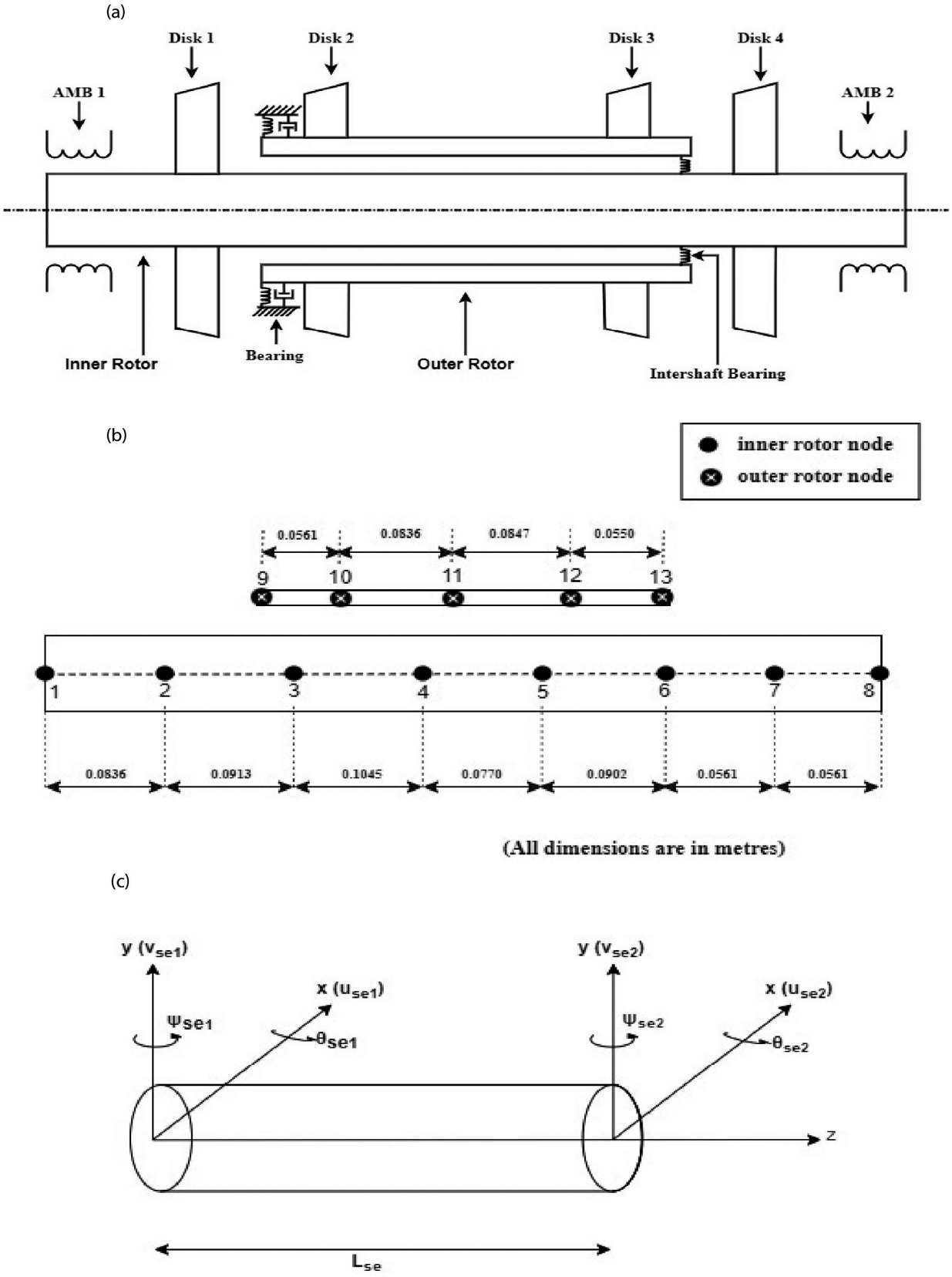

Fig. 2(a) — AMB Coaxial rotor system, (b) discretization of AMBCRS, and (c) local coordinates for the rotor element.

2.2.2 Disk Element

Equation of motion for the rigid disk element is

$$\left[\mathrm{M_{de}}\right]\{\ddot{q}_{de}(t)\}+\Omega\left[G_{\mathrm{de}}\right]\{\dot{q}_{de}(t)\}=\{F_{de}(t)\} \quad \text{... (43)}$$

where, $\left[M_{de}\right]$ and $\left[G_{de}\right]$ are element mass matrix and element gyroscopic matrix respectively, which are given by:

$$[M_{de}]=\begin{bmatrix} m_{de} & 0 & 0 & 0 \\ 0 & m_{de} & 0 & 0 \\ 0 & 0 & I_{de} & 0 \\ 0 & 0 & 0 & I_{de} \end{bmatrix} \quad \text{... (44)}$$

$$[G_{de}]=\begin{bmatrix} 0 & 0 & 0 & 0 \\ 0 & 0 & 0 & 0 \\ 0 & 0 & 0 & I_{pe} \\ 0 & 0 & -I_{pe} & 0 \end{bmatrix} \quad \text{... (45)}$$

2.2.3 Rotor Elements

In the present analysis, the rotors are discretized using Timoshenko beam elements considering both shear as well as rotary inertia effects.[18,19]

The equation of motion for Timoshenko beam element may be expressed as:

$$\left[\mathrm{M_{se}}\right]\{\ddot{q}_{se}(t)\}+\left[\mathrm{K_{se}}\right]\{q_{se}(t)\}=\{F_{se}(t)\} \quad \text{... (46)}$$

where, $\left[\mathrm{M_{se}}\right]$ and $\left[\mathrm{K_{se}}\right]$ in Eq. (46) are given in Appendix.

2.2.4 Solutions of AMB Coaxial rotor system

The generalized displacement *q(t)* in Eq. (36) is

$$q(t)=\{u_1,v_1,\theta_1,\psi_1,u_2,v_2,\theta_2,\psi_2,.....,u_n,v_n,\theta_n,\psi_n\} \quad \text{... (47)}$$

where, *n* is the number of degrees of freedom of the system. For finding out the damped natural frequencies and critical speeds of the AMBCRS, the following 2nd order homogeneous differential equation needs to be solved:

$$[M]\{\ddot{q}(t)\}+[C]\{\dot{q}(t)\}+[K]\{q(t)\}=0 \quad \text{... (48)}$$

Eq. (48) is solved by reducing it into *2n* first order differential equation as

$$\begin{bmatrix}[C] & [M] \\ [M] & 0\end{bmatrix}\frac{d}{dt}\begin{Bmatrix}q(t)\\ \dot{q}(t)\end{Bmatrix}+\begin{bmatrix}[K] & 0 \\ 0 & -[M]\end{bmatrix}\begin{Bmatrix}q(t)\\ \dot{q}(t)\end{Bmatrix}=\begin{Bmatrix}0\\0\end{Bmatrix} \quad \text{... (49)}$$

Eq. (49) in state space form is represented as

$$\begin{bmatrix} C & M \\ M & 0 \end{bmatrix}\{\dot{x}\}+\begin{bmatrix} K & 0 \\ 0 & -M \end{bmatrix}\{x\}=0 \quad \text{... (50)}$$

where,

$$\{\mathrm{x}\}=\begin{Bmatrix} q \\ \dot{q} \end{Bmatrix} \quad \text{... (51)}$$

Eq. (50) is solved by considering the solution of the form

$$\mathrm{x}(\mathrm{t})=x_0\,e^{st} \quad \text{... (52)}$$

Substituting Eq. (52) in Eq. (50), and solving for *s* gives the damped natural frequencies of the AMBCRS. For finding out the steady-state response at nodes of the coaxial rotor system due to the unbalanced force acting on any of the rotor disks, Eq. (36) is modified as:[19]

$$[M]\{\ddot{q}(t)\}+[C]\{\dot{q}(t)\}+\Omega[G]\{\dot{q}(t)\}+[K]\{q(t)\}=\mathrm{Re}\left(\Omega^2 b_0 e^{i\Omega t}\right) \quad \text{... (53)}$$

Eq. (53) is solved for finding out the response of the unbalanced coaxial rotor system.

3 Results and Discussion

Force analysis and multi-objective genetic algorithm (MOGA) described in Section 2 and mathematical model for FEM based rotordynamic analysis (FERDA) presented in Section 3 are applied here for design, analysis and optimization of an active magnetic bearing for the coaxial rotor system shown in Fig. 2(a). MATLAB codes have been developed for the implementation of both FERDA and MOGA. The discretization scheme used here for FERDA is similar to that demonstrated by Friswell *et al.*[19]. The inner and outer rotors are discretized using 7 and 4 Timoshenko beam elements respectively. Each element has 2 nodes and 4 degrees of freedom. Thus the system has 52 degrees of freedom in total. The location of each node is clearly indicated in Fig. 2(b). The values of stiffness and damping coefficient for bearings 2 and 3 are listed in Table 1 while the dimensions and other properties of the coaxial rotor system are given in Table 2. In the present analysis, the coaxial rotor system is assumed to be in contra-rotation with the outer rotor spinning 1.5 times faster than the inner one. Furthermore, both the AMBs are identical and have equal values of stiffness and damping coefficient along *x* and *y* axes. In order to

Table 1 — Bearing properties for preliminary AMBCRS

Bearing	k_{xx} (N/m)	k_{yy} (N/m)	c_{xx} (Ns/m)	c_{yy} (Ns/m)	Node
B1	21×10^6	21×10^6	1718	1718	1
B2	17×10^6	17×10^6	1200	1200	9
B3	9×10^6	9×10^6	1000	1000	6 and 13
B4	21×10^6	21×10^6	1718	1718	8

Table 2 — Disk dimensions for AMBCRS

Disk	Mass (kg)	I_d (kg-m^2)	I_p (kg-m^2)	Node
D1	6	0.0301	0.0602	2
D2	4	0.0149	0.0298	10
D3	1.8	0.0121	0.0242	12
D4	3.5	0.0238	0.0476	7

distribute the gravitational force (weight of the rotor) equally along the two mutually perpendicular load axes of the AMB, it is aligned such that both the load axes are inclined at 45° to the vertical. Hence, the required static load capacity per axis is $87/\sqrt{2} = 62$ N.

The following subsections present the preliminary as well as optimum design results along with a detailed study on the effects of various input parameters on the rotordynamic response of the system.

3.1 Preliminary Design of AMB for Coaxial Rotor System

The six key parameters that govern the performance as well as geometry of an AMB system, i.e. maximum current, pole width, pole length, number of turns, proportional gain and derivative gain are considered as design variables. The description and preliminary values assigned to these variables are given in Table 3. Here the value of maximum current (I_{max}) is estimated using the maximum current density (ζ =6×10^6 A/m^2) and cross-sectional area ($\pi d_c^2/4$) of copper wire. It may be noted that the value of ζ used here is recommended by designers on the basis of thermal considerations.[15,17] Similarly, the preliminary value of N is calculated on the basis of saturation flux density and the value of I_{max} estimated above. The proportional and derivative gains of the PD controller are so chosen that the bearing stiffness and damping coefficient attain reasonable values (Table 1). The representative values assigned to various AMB parameters are listed in Table 4.

Figure 3 presents the Campbell diagram for the coaxial rotor system with AMBs as per the preliminary design specifications given in Table 3. Here the damped natural frequencies of the system are plotted as functions of inner rotor speed. The dashed lines in Fig. 3 represent the correlation between frequency (Hz) and rotational speed (RPM) for inner and outer rotors so that the intersection of these lines

Table 3 — Design Variables

Design Variable	Initial Value	Lower Bound	Upper Bound
No. of turns per pole, N	143	14.3	429
Maximum current, I_{max} (A)	3.02	0.302	9.06
Pole width, w_m (mm)	12.0	1.2	36
Pole length, l, (mm)	10.0	1	30.0
Proportional gain, k_p	15	1.5	45
Derivative gain, k_d	0.0010	0.0001	0.003

Table 4 — AMB Parameters

Parameter	Value
Static load, P_{stat}	$87/\sqrt{2}$ N
Dynamic to static load ratio, γ	5.78
Angular frequency, ω	600π rad/s
Maximum current density of copper wire, ζ	6×10^6 A/m^2
Resistivity of copper wire, ρ	$1.72\times10^{-8}\,\Omega$ m
Diameter of copper wire, d_c	0.8 mm
Maximum voltage across EM circuit, V_p	100 V
Maximum outer diameter of stator, D_{max}	150 mm
Saturation flux density, B_{sat}	1.2 Tesla
Air gap size, G	0.5 mm
Bias indicator, β	6
Half of angle formed by two poles, α	22.5°
Diameter of inner rotor, D_{rot}	40 mm
Sensor gain, G_s	2000 V/m
Amplifier gain, G_d	0.8 A/V
Thickness of the fringes of pole piece, s	1.5 mm
Air gap to core area ratio, c	1.2
Maximum sleeve length, b_{max}	60 mm

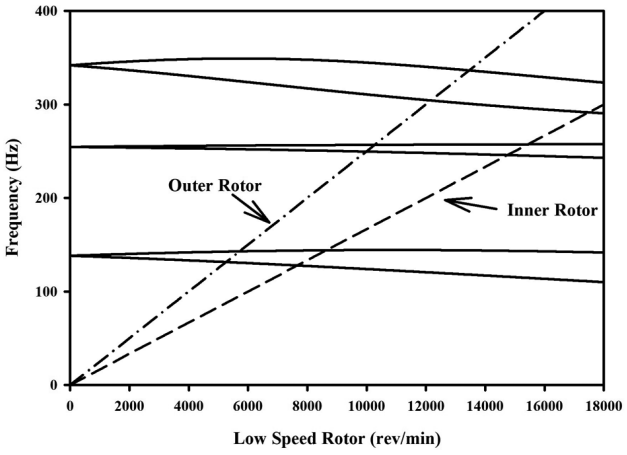

Fig. 3 — Campbell diagram for preliminary AMBCRS.

with the natural frequency plots indicates the rotational speed at which the frequency of unbalanced force equals the natural frequency. It is apparent that, within the speed range considered here, the unbalanced frequency matches with three backward whirl (BW) frequencies at 7617 RPM, 14750 RPM and 17517 RPM along with two forward whirl (FW) frequencies at 8594 and 15343 RPM.

In order to visualize the response of the system for a typical unbalance of 0.0001 kg-m at the disk D1, Fig. 4(a and b) show the variation of vibration amplitudes with respect to inner rotor speed at the locations of the two AMBs and the four disks respectively. These figures reveal two peaks close to the rotational speeds corresponding to 1st FW and 2nd BW mode as deduced from Fig. 3. It is clear from Fig. 4(a) that the first peak crosses the $0.1G$ (=0.05 mm) limit imposed on the maximum amplitude for safe operation of the AMBs. Similarly, as apparent from Fig. 4(b), the maximum amplitude at the location of disk D3 is also quite high. Therefore, the AMB parameters have to be tailored in accordance with all the constraints as demonstrated in the next subsection.

3.2 Optimum Design for Favorable Rotordynamic Response

For obtaining optimized solution using multi-objective genetic algorithm (MOGA), the lower and upper bounds for each design variable are set as 0.1 and 3 times their preliminary values respectively. Hence, search domain for each design variable lies in

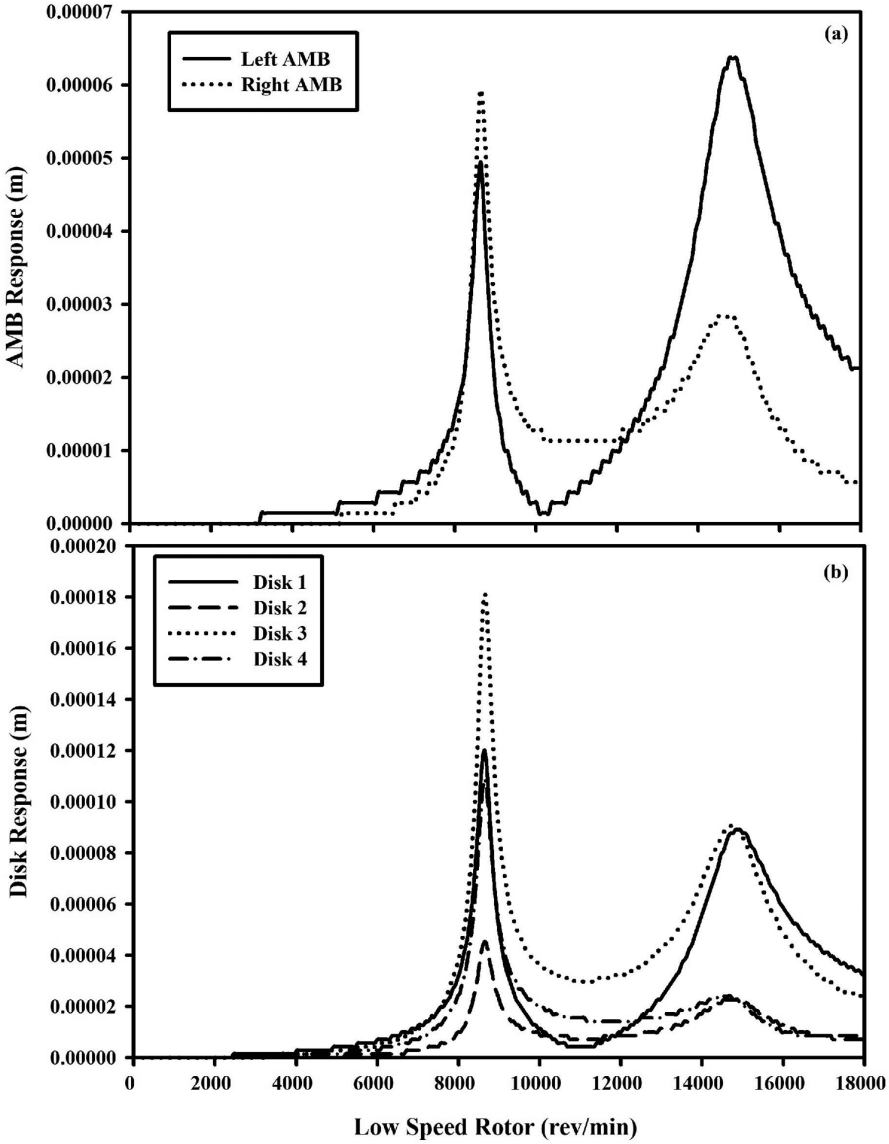

Fig. 4 — Response of AMBCRS for initial design variables at (a) AMBs location, and (b) disks location.

between their corresponding lower and upper bounds. The representative values assigned to various GA parameters are listed in Table 5. The results of the GA based search for the values of design variables to maximize the force slew rate limitation and minimize the overall bearing volume subject to various constraints are compiled in Table 6. The overall bearing volume is found to decrease by 720.02 cm^3 with respect to its preliminary design value. The optimization scheme is so implemented that it ensured maximum satisfaction of all the constraints. It has been achieved at the expense of force slew rate limit which is slightly lower than that for preliminary design. It may be noted that most of the constraints were not satisfied for the case of preliminary design.

In order to visualize the effectiveness of optimization procedure, Fig. 5(a) clearly indicates

Table 5 — Parameters in Genetic Algorithm

Parameter	Value
Population size (constant), n_{popu}	120
Number of generations, n_{gen}	120
Number of bits in the binary code, n_{bit}	16
Cross-over probability, p_c	1
Mutation probability (Variable), p_m	0 - 0.4

Table 6 — Design Results

Design Variable	Final Value
No. of turns per pole, N	219
Maximum current, I_{max} (A)	2.33
Pole width, w_m (mm)	17.42
Pole length, l, (mm)	18.19
Proportional gain, k_p,	17.305
Derivative gain, k_d	0.0017
Sleeve thickness, w (mm)	17.41
Objective 1: Force slew rate, $\hat{P}$ (kN/s)	523.4
Objective 2: Bearing volume, V_{brg} (cm^3)	717.18
Diameter of the stator, D_{stator} (mm)	150.07
Sleeve length, b (mm)	40.53
Stator thickness, t_s (mm)	17.42
Maximum copper loss, P_{Cu} (W)	9.42

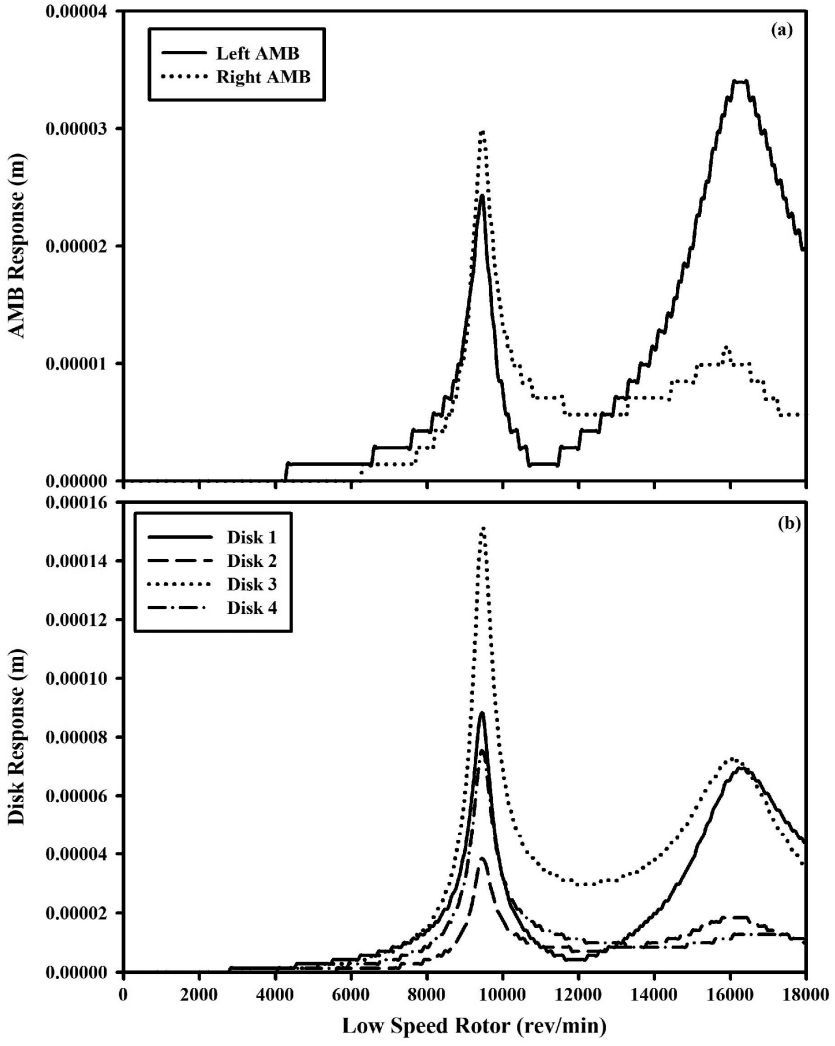

Fig. 5 — Response of AMBCRS for optimized design variables at (a) AMBs location, and (b) disks location.

that the vibration amplitudes at the location of AMBs are reduced to acceptable values, i.e., below 0.1*G* (=0.05 mm). Besides, the maximum amplitude observed for the case of D3 drops from 0.181 mm (Fig. 4(b)) to 0.149 mm (Fig. 5(b)). Also, amplitude of vibration at the unbalance disk D1 drops from 0.121 mm (Fig. 4(b)) to 0.089 mm (Fig. 5(b)). Hence, it follows that the stiffness and damping properties of an AMB can be easily tailored as per the desired rotordynamic behavior by designing its controller and actuator accordingly – one of the major advantages of AMBs over the conventional bearings.

Figure 6 shows the Campbell diagram pertaining to the optimized AMBCRS. It is found that the damped natural frequencies exist in pair for the case of 0 RPM due to identical bearing stiffness in x and y directions and absence of coupling between two transverse planes. Further on comparison with Fig. 3, it follows that critical speeds are shifted towards higher rotational speed in comparison to the preliminary design.

3.3 Effect of Unbalance on AMB Parameters

Dynamic load plays a crucial role in the design of an AMB and the most common source of synchronous dynamic load is the mass unbalance. In case, the mass unbalance in a rotor system exceeds the design value, the AMB hardware will have to be re-designed. Therefore, from a designer's viewpoint, it is important to study effects of mass unbalance on AMB actuator parameters affecting the hardware components of the system, i.e., maximum current, pole length, pole width, and number of turns. The optimum values of these parameters for four magnitudes of mass unbalance are compared in Fig. 7.

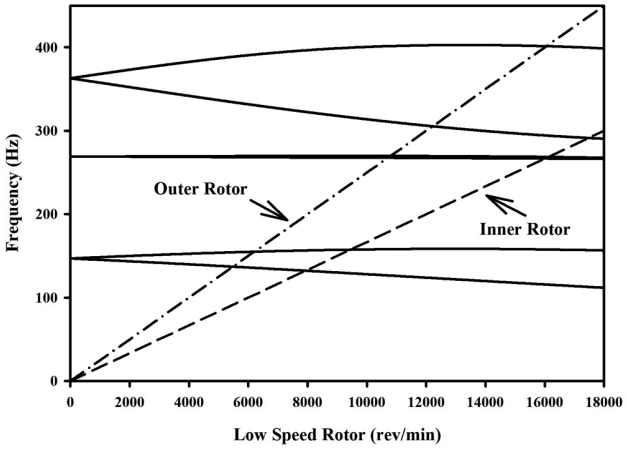

Fig. 6 — Campbell diagram for optimized AMBCRS.

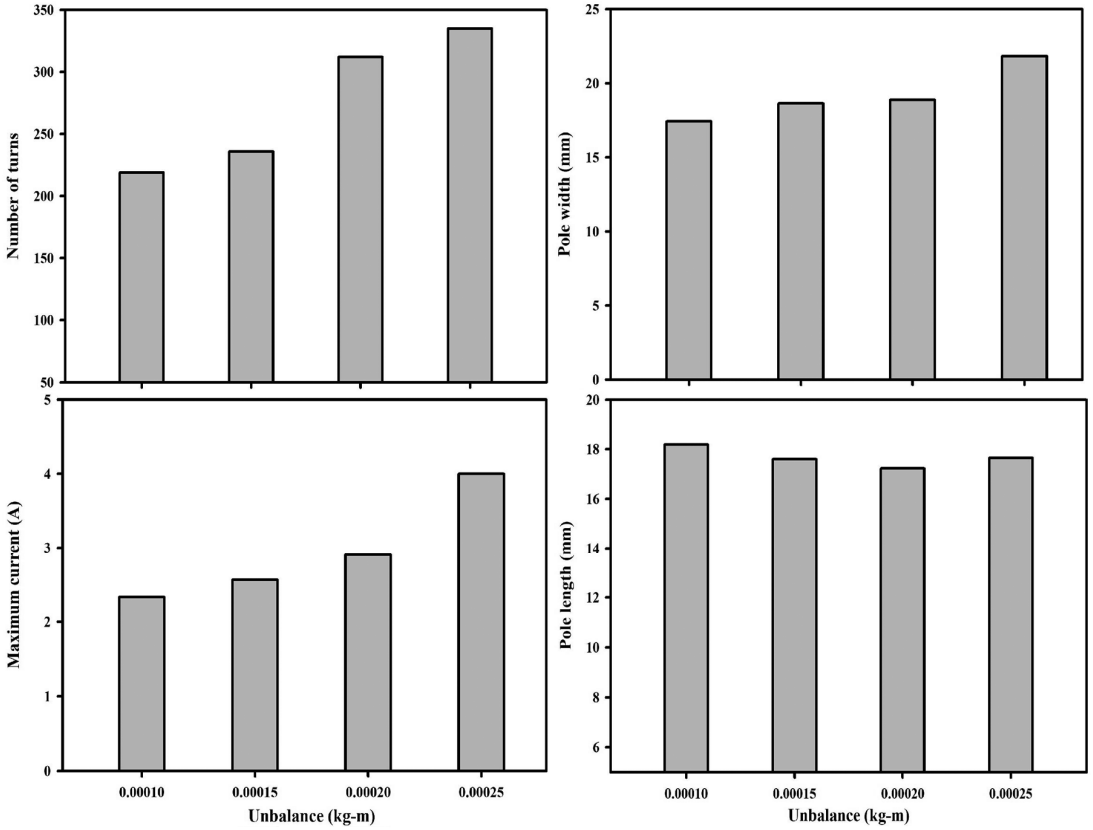

Fig. 7 — Effect of unbalance on AMB parameters.

It can be seen that as the unbalance on the disk D1 increases from 0.0001 kg-m to 0.00025 kg-m, the number of turns increases from 219 to 335 while the pole width increases from 17 mm to 22 mm. Similarly, maximum current also increases from 2.33A to 4A, however, the pole length remains almost unchanged.

4 Conclusion

Finite element based rotordynamic analysis of AMBCRS and optimization of AMB parameters (pole width, number of turns, maximum current, pole length, proportional gain and derivative gain) using multi-objective genetic algorithm (MOGA) have been carried out. Based on the results presented in the previous section, the following conclusions are drawn:

- The effect of optimization on the dynamic response of the unbalanced coaxial rotor system has been investigated. With optimized design parameters, the maximum amplitude of vibration at the locations of the AMBs could be contained within 10% of the air gap. Under the present conditions, the peak amplitudes at the AMB and the disk D3 are found to decrease by 46.9% and 17.68% respectively. Also, a decrement of 26.5% in amplitude at unbalance disk D1 has been achieved as a result of optimization.
- The proportional and derivative gains of the controller are found to govern the stiffness and damping characteristics of the AMBs. However, an arbitrarily designed controller may not ensure safe operation of the system. Therefore, a systematic optimization procedure like the one presented herein is necessary.
- Mass unbalance is the major source of synchronous vibrations in a rotor system. For an increase in mass unbalance from 0.0001 kg-m to 0.00025 kg-m, the optimum values of number of turns, pole width and maximum current are found to increase by 52.9%, 29.4% and 71.67% respectively. Although, pole length remains constant throughout possibly because of its optimized value and non-violation of constraint imposed on the stator diameter and winding space.
- Touch-down bearings are used in AMB rotor systems for the protection of active magnetic bearings and other system components during failure. This work offers a useful tool for designing the touch-down bearings for an AMB system.
- The maximum current is governed by the maximum allowable current density through the winding wire and its diameter. Under the present operating and geometric conditions, the current required to carry the static and dynamic load is close to its maximum allowable limit and hence, an increase in mass unbalance does not cause any noticeable change in its value till 0.0002 kg-m. But with further increase in mass unbalance, maximum current reaches its saturation condition which results in sudden increase in its value.

References

1 Chiang H W D, Hsu C N, & Tu S H, *J Propuls Power*, 20 (2004) 1096.
2 Ferraris G, Maisonneuve V, & Lalanne M, *J Sound Vib*, 195 (1996) 649.
3 Yang Y, Cao D, Yu T, Wang D, & Li C, *Int J Mech Sci*, 115 (2016) 253.
4 Schweitzer G & Maslen H, *Magnetic Bearings: Theory, Design, and Application to Rotating Machinery*, (Springer-Verlag, Berlin), 2009.
5 Bornstein K R, *J Tribol*, 113 (1991) 598.
6 Samanta P & Hirani H, *IEEE Trans Magn*, 44 (2008) 292.
7 Lijesh K P, Doddamani M, & Bekinal S I, *J Tribol*, 140 (2018) 021901.
8 Kuppa S K & Lal M, *J Verif Valid Uncertain Quantif*, 4 (2019) 031001.
9 Srinivas R S, Tiwari R, & Babu C K, *J Dyn Syst Meas Control*, 143 (2020) 011007.
10 Zhao Y, Yang G, Keogh P, & Zhao L, *J Tribol*, 139 (2017) 041701.
11 Yulan Z, Xingnan L, Guojun Y, Zhengang S, & Lei Z, *J Tribol*, 140 (2018) 041704.
12 Barbosa Moreira A B & Thouverez F, *J Eng Gas Turbines Power*, 142 (2020) 041004.
13 Rao J S & Tiwari R, *Int J Comput Methods Eng Sci Mech*, 9 (2008) 223.
14 Zhong W & Palazzolo A, *J Dyn Syst Meas Control*, 137 (2015) 021012.
15 Lijesh K P & Hirani H, *J Tribol*, 137 (2015) 024502.
16 Zhong W, Palazzolo A, & Kang X, *J Vib Acoust*, 139 (2017) 011011.
17 Hsiao F Z, Fan C C, Chieng W H, & Lee A C, *JSME Int J Ser C*, 39 (1996) 586.
18 Nelson H D, *J Mech Design*, 102 (1980) 793.
19 Friswell M I, Penny J E T, Garvey S D, & Lees A W, *Dynamics of Rotating Machines*, (Cambridge University Press, Cambridge), 2010.